




Repurposing of FDA-approved antivirals, antibiotics, anthelmintics, antioxidants, and cell protectives against SARS-CoV-2 papain-like protease

Mahmoud Kandeel^{a,b}, Alaa H. M. Abdelrahman^c, Kentaro Oh-Hashi^d, Abdelazim Ibrahim^e, Katharigatta N. Venugopala^{f,*}, Mohamed A. Morsy^{f,#} and Mahmoud A. A. Ibrahim^c 

^aDepartment of Biomedical Sciences, College of Veterinary Medicine, King Faisal University, Al-ahsa, Saudi Arabia; ^bDepartment of Pharmacology, Faculty of Veterinary Medicine, Kafrelshikh University, Kafrelshikh, Egypt; ^cComputational Chemistry Laboratory, Chemistry Department, Faculty of Science, Minia University, Minia, Egypt; ^dDepartment of Chemistry and Biomolecular Science, Faculty of Engineering, Gifu University, Gifu, Japan; ^eDepartment of Pathology, College of Veterinary Medicine, King Faisal University, Al-ahsa, Saudi Arabia; ^fDepartment of Pharmaceutical Sciences, College of Clinical Pharmacy, King Faisal University, Al-Ahsa, Saudi Arabia

Communicated by Ramaswamy H. Sarma

ABSTRACT

SARS-CoV-2 or Coronavirus disease 19 (COVID-19) is a rapidly spreading, highly contagious, and sometimes fatal disease for which drug discovery and vaccine development are critical. SARS-CoV-2 papain-like protease (PL^{PRO}) was used to virtually screen 1697 clinical FDA-approved drugs. Among the top results expected to bind with SARS-CoV-2 PL^{PRO} strongly were three cell protectives and antioxidants (NAD⁺, quercitrin, and oxiglutatione), three antivirals (ritonavir, moroxydine, and zanamivir), two antimicrobials (doripenem and sulfaguandine), two anticancer drugs, three benzimidazole anthelmintics, one antacid (famotidine), three anti-hypertensive ACE receptor blockers (candesartan, losartan, and valsartan) and other miscellaneous systemically or topically acting drugs. The binding patterns of these drugs were superior to the previously identified SARS CoV PL^{PRO} inhibitor, 6-mercaptopurine (6-MP), suggesting a potential for repurposing these drugs to treat COVID-19. The objective of drug repurposing is the rapid relocation of safe and approved drugs by bypassing the lengthy pharmacokinetic, toxicity, and preclinical phases. The ten drugs with the highest estimated docking scores with favorable pharmacokinetics were subjected to molecular dynamics (MD) simulations followed by molecular mechanics/generalized Born surface area (MM/GBSA) binding energy calculations. Phenformin, quercetin, and ritonavir all demonstrated prospective binding affinities for COVID-19 PL^{PRO} over 50 ns MD simulations, with binding energy values of -56.6 , -40.9 , and -37.6 kcal/mol, respectively. Energetic and structural analyses showed phenformin was more stable than quercetin and ritonavir. The list of the drugs provided herein constitutes a primer for clinical application in COVID-19 patients and guidance for further antiviral studies.

ARTICLE HISTORY

Received 7 June 2020
Accepted 13 June 2020

KEYWORDS

COVID-19; molecular dynamics; SARS-CoV-2; PL^{PRO}; protease



Introduction


SARS-CoV-2 or Coronavirus disease-19 (COVID-19) has recently emerged in China and rapidly spread throughout many other countries (WHO, 2020). The new SARS-CoV-2 was classified as a Beta-coronavirus (Liu et al., 2020). As recently evolved, there is a great demand for the discovery of new drugs against SARS-CoV-2.

The new SARS-CoV-2 is classified as a beta-coronavirus (Liu et al., 2020), characterized by a large genome of approximately 30 kb, and comprised of genes for four structural proteins—spike (S), envelop (E), membrane (M), and nucleocapsid (N)—and non-structural (NS) genes (Shi et al., 2015). In CoVs, there are 14–16 NS genes encoding proteins used in the vital processes of virus genomic transcription, protein processing, virion assembly, and replication (Brian &

Baric, 2005). CoV infections caused mild respiratory symptoms until more dangerous forms evolved approximately two decades ago, noted by the emergence of SARS CoV. Three highly fatal CoVs have been of global health concern: SARS CoV, MERS CoV, and SARS-CoV-2 (Guarner, 2020). The SARS-CoV-2 genome composition is highly similar to that of SARS CoV, yet the former possesses inherently more efficient gene expression due to more biased codon usage and lower effective codon numbers than SARS CoV, pangolin Beta-CoV, bat SARS CoV, and MERS CoV (Kandeel et al., 2020; Kandeel & Altaher, 2017).

The CoV NS polyprotein is processed by two proteases, the main protease (Mpro) (a strict protease) and the multifunctional PL^{PRO} (Harcourt et al., 2004). Inhibition of PL^{PRO} impacts virus replication via deficient viral protein processing and can also affect remote PL^{PRO} activities, including

CONTACT Mahmoud Kandeel  mkandeel@kfu.edu.sa  Department of Biomedical Sciences, College of Veterinary Medicine, King Faisal University, Al-hofuf, Al-ahsa, 31982, Saudi Arabia

 Supplemental data for this article can be accessed online at <https://doi.org/10.1080/07391102.2020.1784291>.

*Department of Biotechnology and Food Technology, Durban University of Technology, Durban 4001, South Africa.

#Department of Pharmacology, Faculty of Medicine, Minia University, 61511 El-Minia, Egypt

© 2020 Informa UK Limited, trading as Taylor & Francis Group

deubiquitination, de-ISGylation, and innate, anti-host immunity reactions (Báez-Santos et al., 2014; Mielech et al., 2014). PL^{PRO} comprises a central catalytic domain and the ubiquitin-like domain (Ubl) (Bailey-Elkin et al., 2014; Lei et al., 2014; Yang et al., 2014), which interferes with the host IRF3 and NF-κB antiviral pathways and modulates the host immune response (Ratia et al., 2014). PL^{PRO} subdomains showed different reaction patterns in the presence or absence of ubiquitin (Alfuwaires et al., 2017b). Furthermore, PL^{PRO} was an important drug target against several CoVs, including MERS CoV (Kandeel et al., 2019) and SARS CoV (Báez-Santos et al., 2015).

FDA-approved drugs are the first potential treatments to use in emergent cases, due to their commercial availability, proven safety, and direct applicability without the need for any preclinical and clinical testing. This study aims to identify the top candidates among FDA-approved drugs with strong binding potential for SARS-CoV-2 PL^{PRO}, with the ultimate goal of repurposing drugs for inhibition of SARS-CoV-2. The most promising drugs based on the predicted docking scores for COVID-19 PL^{PRO} will be further investigated using molecular dynamics simulations over 50 ns. A molecular mechanics/generalized Born surface area (MM/GBSA) approach will be applied to evaluate drug- PL^{PRO} binding energies ($\Delta G_{\text{binding}}$) throughout the MD simulated time. The stability, binding affinity, and interactions of the drug-PL^{PRO} binding will also be estimated.

Methods

Construction of FDA-approved drugs dataset

A dataset of FDA-approved drugs was obtained as an SDF file from Selleckchem Inc. (WA, USA). The drugs dataset was imported to the ligprep module of the Maestro package (Schrodinger Inc., LLC, NY, USA). The structures of drugs were 3D optimized at neutral pH and desalted.

Preparation of SARS-CoV-2 PL^{PRO} structure

The structure of SARS-CoV-2 PL^{PRO} was retrieved from the protein data bank (PDB ID 6w9c) and imported to the protein preparation module in the Maestro software package. Protein preparation was as previously described (Alfuwaires et al., 2017a; Kandeel et al., 2020; Kandeel & Al-Nazawi, 2020). Briefly, the protein was preprocessed to assign the substructure components and detect potential errors. The structure was protonated and optimized at neutral pH. The protein structure was energy minimized using an OPLS2005 force field. The docking grid was generated by selecting the co-crystallized ligand, and the grid box extended to approximately 20 Å around the ligand.

Virtual screening

Virtual screening was implemented by the glide docking module of the Maestro package using the standard precision (SP docking) mode (Friesner et al., 2004). 6-Mercaptopurine

(6-MP) was proved to be a potent inhibitor of SARS PL^{PRO} with $IC_{50} = 0.0216 \mu\text{M}$ (Báez-Santos et al., 2015). The result of the docking run was compared to the values of 6-MP as a reference inhibitor.

Molecular dynamics simulations

Molecular dynamics (MD) simulations were conducted on the most promising drugs to target PL^{PRO} using AMBER16 software (Case et al., 2016). In MD simulations, the general AMBER force field 2 (GAFF2) ("GAFF and GAFF2 are public domain force fields and are part of the AmberTools16 distribution, a.f.d.a.h.a.o.i.a.A.M.A.t.") and AMBER force field (Maier et al., 2015) were utilized to describe drugs and COVID-19 PL^{PRO}, respectively. The restrained electrostatic potential (RESP) approach (Bayly et al., 1993) at the HF/6-31G* level was employed to estimate the atomic partial charges of the drugs. The quantum mechanical calculations were conducted using Gaussian09 software (Frisch et al., 2009). The docked drug- PL^{PRO} complexes were solvated in a cubic water box with 15 Å distances between the edges of the box and any atom of the complexes. The solvated complexes were then minimized for 5000 steps and gently annealed from 0 K to 300 K over 50 ps. The systems were equilibrated for 1 ns, and production stages were executed over simulation times of 50 ns. Every 10 ps, a snapshot was taken over the production stage, giving 5,000 snapshots for each complex. Periodic boundary conditions and the NPT ensemble were adopted in all explicit MD simulations, including both the equilibration and production stages. Long-range electrostatic interactions under periodic conditions were treated with the Particle Mesh Ewald (PME) method (Darden et al., 1993) with a direct space cut-off of 12 Å. The temperature was held constant at 298 K using Langevin dynamics with the gamma_In parameter set to 1.0. A Berendsen barostat with a relaxation time of 2 ps was employed to control system pressure (Berendsen et al., 1984). All bonds involving hydrogen atoms were constrained using the SHAKE option, and the time step was set to 2 fs. The MD simulations were executed with the GPU version of pmemd (pmemd.cuda) in AMBER16 on the CompChem GPU/CPU cluster (hpc.compchem.net).

Binding energy calculations

Coordinates and energy values were collected every 10 ps over the production stage for binding energy calculations. Based on the collected coordinates, the binding energies of the drugs with COVID-19 PL^{PRO} were evaluated using the molecular mechanics-generalized Born surface area (MM-GBSA) approach (Massova & Kollman, 2000). The MM-GBSA binding free energies were estimated as follows:

$$\Delta G_{\text{binding}} = G_{\text{Complex}} - (G_{\text{drugs}} + G_{\text{PLpro}})$$

where the energy term (G) is estimated as:

$$G = E_{\text{vdw}} + E_{\text{ele}} + G_{\text{GB}} + G_{\text{SA}}$$

with E_{vdw} , E_{ele} , G_{GB} and G_{SA} as the van der Waals, electrostatic, General Born solvation, and surface area energies,

respectively. Entropy contributions were not considered in this study.

Statistical analysis

Several correlation runs were conducted to evaluate the relation between the calculated docking score and the functional parameters of compounds recognition by SARS-CoV-2 PL^{PRO}. Pearson's correlation coefficient and the significance degree were estimated in GraphPad Prism software.

Results

The virtual screening results of a total of 1697 FDA-approved drugs against the SARS-CoV-2 PL^{PRO} are provided in [Supplementary File 1](#). The presented parameters include the docking scores, ligand efficiencies, and lipophilic and hydrogen bonding interactions. [Table 1](#) shows the compounds with the highest docking scores, including 26 compounds with a docking score of -7 or higher. The relative docking score and interaction parameters were calculated based on the values of the reference PL^{PRO} inhibitor 6-mercaptopurine (6-MP).

Among the top hits ([Table 1](#) and [Figure 1](#)), there were three general tonics, cell-protective substances, and antioxidants (NAD⁺, quercetin, and oxyglutathione), three antivirals (ritonavir, moroxydine, and zanamivir), two antimicrobials (doripenem and sulfaguandine), two anticancer drugs, three anthelmintics from the benzimidazole group, one antacid (famotidine), and other miscellaneous systemically or topically acting drugs.

As shown in [Supplementary File 1](#), 6-MP occupied the 132nd rank in the virtual screening study. Therefore, the top retrieved hits were more likely to have more potent interactions with SARS-CoV-2 PL^{PRO}. The improved docking scores were derived by a corresponding increase in both the hydrophobic scores and hydrogen bonding interactions.

To analyze the interactions of the top hits in comparison with the reference drug, the ligand interaction profiles of drugs and the analyses of the contributing forces were plotted ([Figure 1](#)). The binding mode of the compounds showed a U-shaped configuration ([Figure 2](#)); it had a U-shaped cavity with the arms of the U hosting TYR261. Zanamivir formed three hydrogen bonds with ASP157, GLU160, and TYR261. NAD⁺ showed a strong network of five hydrogen bonds, one salt bridge, and stacking interactions. Ritonavir showed four hydrogen bonds and a stacking interaction with ARG159 ([Figure 3](#)).

Statistical analysis revealed a significant positive correlation between the docking score and the hydrogen bonds, lipophilic interactions, and ligand efficiency scores ($p < .001$) ([Table 2](#)). The molecular weight did not show a significant correlation with the docking score. The positive correlation between both the hydrogen bond and the Glide lipo confirms the role of both hydrogen bonding and lipophilic interactions in the binding to PL^{PRO}. This contributed to the improved docking scores of the top hits compared with the score of the previously identified PL^{PRO} inhibitor 6-MP.

Molecular dynamics simulation

Conformational flexibilities of drug-receptor complexes, solvent effects, and dynamics must be determined to attain dependable drug-receptor-binding affinities (De Vivo et al., 2016; Kerrigan, 2013). Therefore, molecular dynamic (MD) simulations combined with binding energy (MM-GBSA) calculations over 50 ns were conducted for the most promising drugs (i.e. those which had predicted docking scores in association with COVID-19 PL^{PRO}). The evaluated average MM-GBSA binding energies over the 50 ns MD simulations are listed in [Table 3](#). According to the calculated MM-GBSA binding energies ($\Delta G_{binding}$), only 3 of the 10 investigated drugs demonstrated considerable binding energies ($\Delta G_{binding} > -37.6$ kcal/mol); 7 exhibited relatively weak binding energies in the range of $-36.4 \geq \Delta G_{binding} \geq -19.5$. Interestingly, phenformin, quercetin, and ritonavir showed promising binding affinities toward COVID-19 PL^{PRO}, with binding energies ($\Delta G_{binding}$) of -56.5 , -40.9 , and -37.6 kcal/mol, respectively ([Table 4](#)).

Post-dynamics analyses

Binding energy decomposition

Decomposition of the average MM-GBSA binding energy over a 50 ns MD simulation was carried out to disclose the nature of dominant interactions for phenformin, quercetin, and ritonavir with COVID-19 PL^{PRO} ([Table 2](#)). According to energy decomposition results, the electrostatic interactions (E_{ele}) were the dominant forces in the drug-PL^{PRO} binding affinity, with values of -124.1 , -75.0 , and -26.7 kcal/mol for the phenformin-PL^{PRO}, quercetin-PL^{PRO}, and ritonavir-PL^{PRO} complexes, respectively. In addition, the van der Waals (E_{vdw}) contributions were favorable, with values of -23.2 , -33.5 , and -45.0 kcal/mol for the phenformin-PL^{PRO}, quercetin-PL^{PRO}, and ritonavir-PL^{PRO} complexes, respectively.

Hydrogen bond length

Correlational analyses of the hydrogen bond lengths between phenformin, quercetin, and ritonavir and the key amino acid ASP157 residue were estimated through 50 ns MD simulations and are presented in [Figure 4a](#). What stands out in the figure is the higher stability of phenformin and ritonavir inside the active site of COVID-19 PL^{PRO}, with average hydrogen bond lengths of 2.10 and 2.29 Å, respectively. Quercetin formed a stable hydrogen bond through the first 30 ns, with an average length of 1.70 Å. After 30 ns in the MD simulations, there was an increase in the hydrogen bond length, however, so that the average bond length was 2.92 Å throughout the final 20 ns of the MD time.

Center-of-mass distance

Phenformin, quercetin, and ritonavir inside the active site of COVID-19 PL^{PRO} were further scrutinized by measuring the center-of-mass (CoM) distance between the drug and the ASP157 residue through the 50 ns of the MD simulations (see

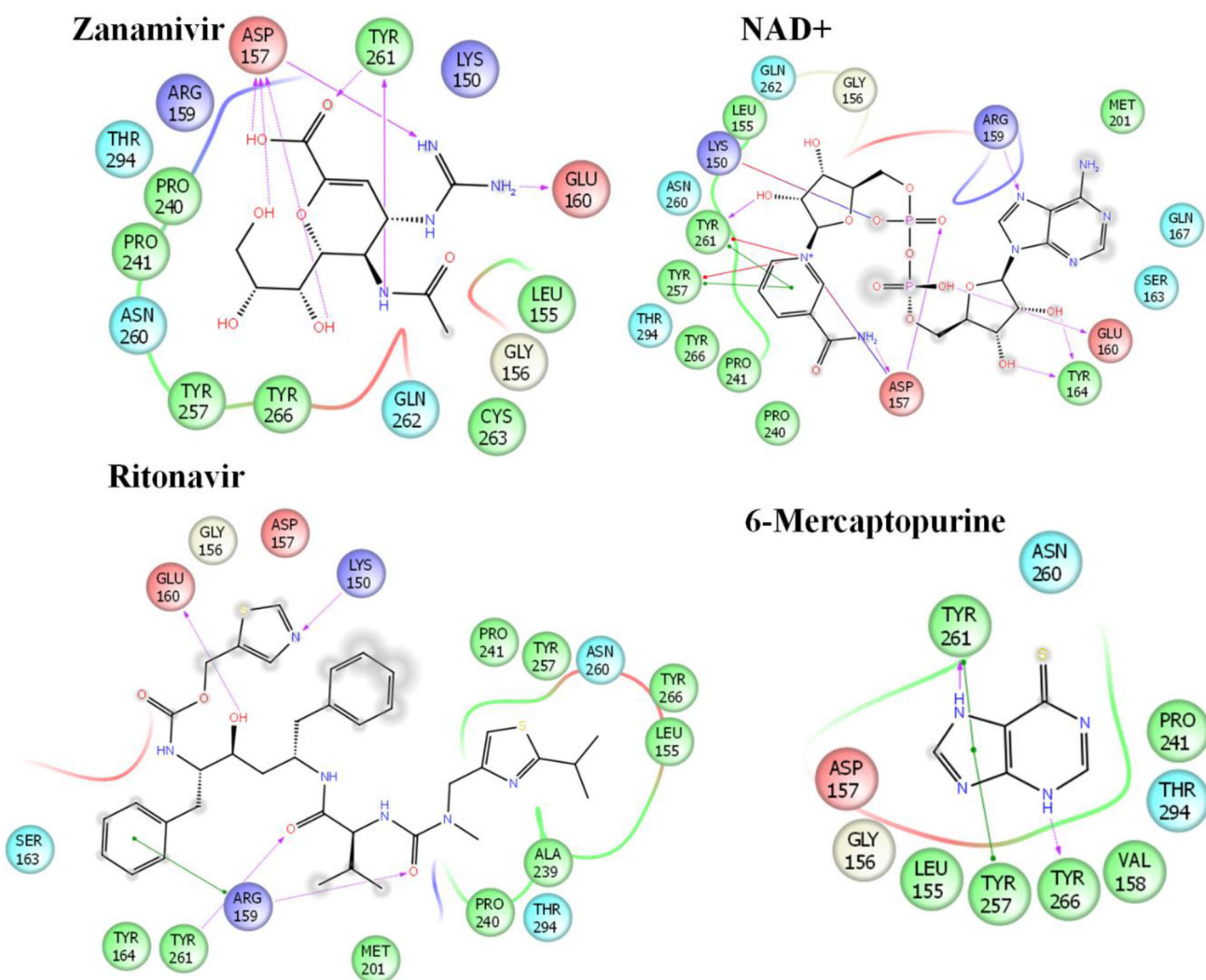


Figure 3. The ligand interactions of zanamivir, NAD⁺, ritonavir, and 6-mercaptopurine with SARS-CoV-2 PL^{pro}. Charged residue (negative) in pink, positive charged residue in blue, and hydrophobic residues in cyan; hydrogen bonds indicated by purple arrow; stacking interactions indicated by green lines.

Table 2. Pearson's correlation of the obtained docking score with the drug's molecular weight and interaction parameters with SARS-CoV-2 PL^{pro}.

	Docking score vs. glide ligand efficiency	Docking score vs. glide lipo	Docking score vs. glide hbond	Docking score vs. MolWeight
Pearson r	0.3024	0.2311	0.3602	0.01789
95% confidence interval	0.2585 to 0.3451	0.1855 to 0.2757	0.3181 to 0.401	-0.02978 to 0.06547
R squared	0.09147	0.05341	0.1298	0.00032
P value				
P (two-tailed)	<0.0001	<0.0001	<0.0001	0.4620
P value summary	****	****	****	ns
Significant? (alpha = 0.05)	Yes	Yes	Yes	No
Number of XY Pairs	1693	1693	1693	1693

Table 3: Calculated MM-GBSA binding energies (in kcal/mol) for the top 10 potent drugs against COVID-19 PL^{pro} over 50 ns MD simulations.

No.	Drug name	MM-GBSA Binding energy (kcal/mol)
1	Phenformin	-56.5
2	Quercetin	-40.9
3	Ritonavir	-37.6
4	Montelukast	-36.4
5	Fosmatinib1	-33.5
6	Nadid	-32.9
7	Candestran	-28.9
8	Valsartan	-28.6
9	Zanamivir	-24.7
10	Oxyglutathione	-19.5

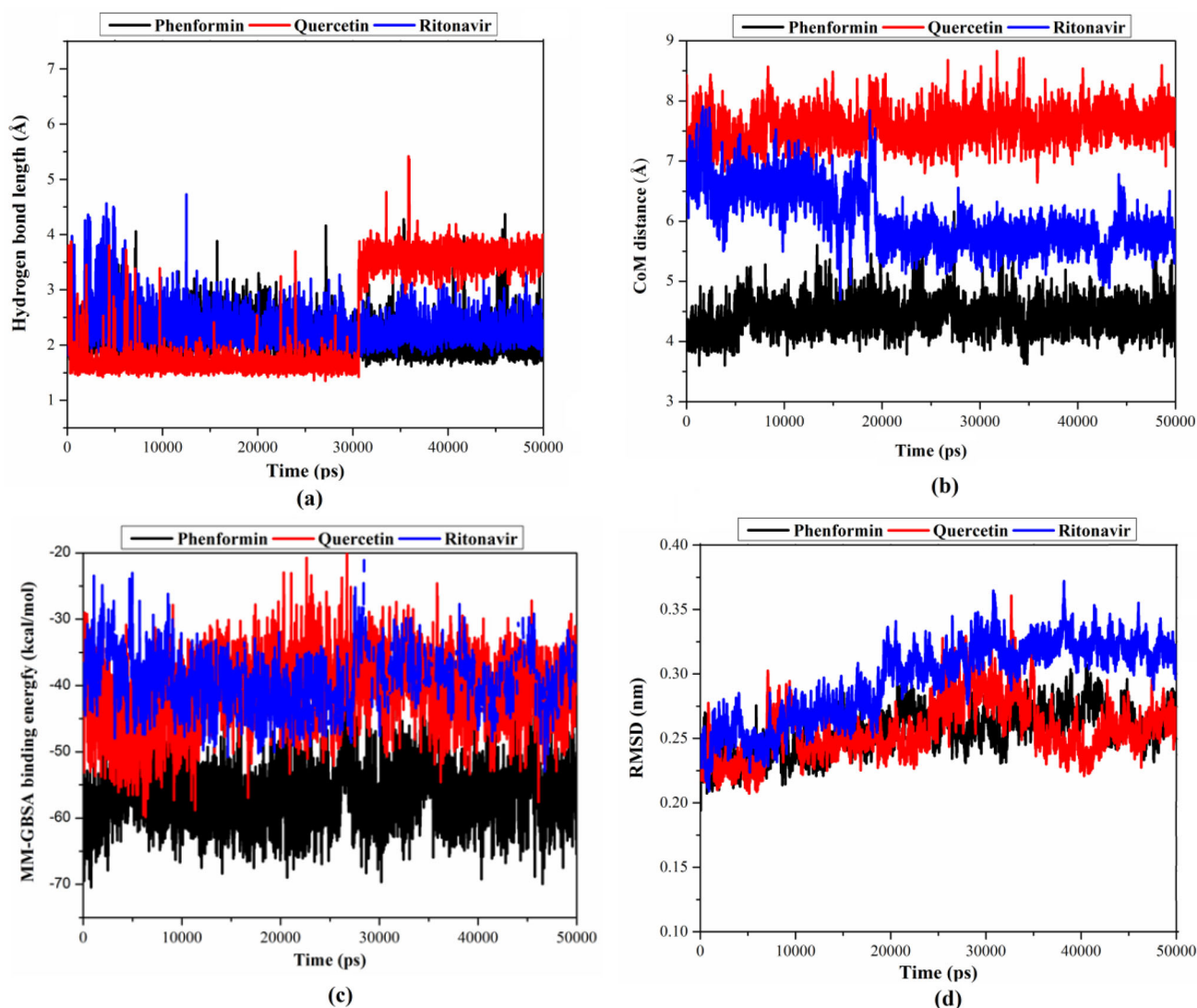
Figure 4b). The CoM distance data in **Figure 4b** demonstrate that phenformin, quercetin, and ritonavir showed high stability inside the active site of COVID-19 PL^{pro} during the 50 ns of the MD simulations, with average CoM distances of 4.55, 7.57, and 6.05 Å, respectively.

Binding energy per frame

Correlations between the binding energy and time would grant a deeper insight into the stability of the drug-PL^{pro}

Table 4. Decomposition of MM-GBSA binding energies for phenformin, quercetin and ritonavir in complex with COVID-19 PL^{PRO} through 50 ns MD simulations.

Drug Name	Calculated MM-GBSA binding energy (kcal/mol)						
	ΔE_{VDW}	ΔE_{ele}	ΔE_{GB}	ΔE_{SUR}	ΔG_{gas}	ΔG_{Solv}	$\Delta G_{binding}$
Phenformin	-23.2	-124.1	94.8	-4.0	-147.3	90.7	-56.5
Quercetin	-33.5	-75.0	72.7	-5.2	-108.4	67.6	-40.9
Ritonavir	-45.0	-26.7	40.0	-5.9	-71.7	34.0	-37.6

**Figure 4.** (a) Hydrogen bond lengths. (b) CoM distances between the most promising drugs and the key residue amino acid ASP157. (c) Variations in the MM-GBSA binding energies. (d) RMSD of the backbone atoms from the initial structure for phenformin (black), quercetin (red), and ritonavir (blue) in complex with PL^{PRO} through 50 ns MD simulations.

interactions. The MM-GBSA binding energies were therefore measured per frame for phenformin, quercetin, and ritonavir with PL^{PRO} and are displayed in Figure 4c. Data in Figure 4c revealed that the phenformin, quercetin, and ritonavir complexes demonstrated a tight binding affinity over the 50 ns of the MD, with an average $\Delta G_{binding}$ of -56.5, -40.9, and -37.6 kcal/mol, respectively. These findings show a promising stability of phenformin, quercetin, and ritonavir in complex with PL^{PRO} over the simulated MD time of 50 ns.

Root-mean-square deviation

The root-mean-square deviation (RMSD) was utilized to scrutinize the structural changes in the drug-PL^{PRO} complexes over the MD simulated time. The RMSD for the backbone atoms of phenformin, quercetin, and ritonavir in complex with PL^{PRO} relative to the starting structures throughout the 50 ns MD simulations were estimated and are summarized in Figure 4d. What stands out in this figure is the backbone of the phenformin-, quercetin-, and ritonavir-PL^{PRO} complexes and the demonstrated stability over the 50 ns MD

simulations, giving an RMSD of less than 0.35 nm. Overall, these results indicate that the three investigated drugs are tightly bonded in the active site of the PL^{PRO} and do not impact the overall topology of the PL^{PRO}.

Discussion

This work covers an essential gap in the discovery of new drugs against COVID-19. CoVs encode a limited number of virus-encoded enzymes. Therefore, the therapeutic opportunities are directed to these targets in the hope of finding new anti-SARS drugs. Of these enzymes, PL^{PRO} lies at the heart of drug discovery targets owing to its essential function in processing the viral polyprotein, as well as its multiple remote activities that lead to suppression of the host immune response.

In criticizing the top hits, some of these drugs are not suitable for oral administration due to pharmacokinetic restrictions, for example, because of the poor absorption of sulfaguanidine and most of the benzimidazole anthelmintics. Others have important effects on body system functions, such as tezacaftor (cystic fibrosis), guanabenz (adrenoceptor agonist), venetoclax and taxifolin (anticancer drugs), and chlorhexidine (a drug for topical application).

Three previously known antivirals were found among the top hits (ritonavir, moroxydine, and zanamivir). Ritonavir is a viral protease inhibitor approved for treating HIV (Croxtall & Perry, 2010). Ritonavir/lopinavir was successful in treating an index case with severe pneumonia (Lim et al., 2020). Moroxydine is an old antiviral with several new derivatives that are effective against the hepatitis C virus (Magri et al., 2015). It has broad-spectrum antiviral actions involving DNA and RNA viruses (Yu et al., 2016, 2018). Zanamivir is a strong influenza neuraminidase inhibitor (Zhao et al., 2017). It is used in combination with oseltamivir for treating drug-resistant H1N1 influenza (de Mello et al., 2018).

Three previously known antivirals were found among the top hits (ritonavir, moroxydine, and zanamivir). Ritonavir is a viral protease inhibitor approved for treating HIV (Croxtall & Perry, 2010). Ritonavir/lopinavir was successful in treating an index case with severe pneumonia (Lim et al., 2020). Moroxydine is an old antiviral with several new derivatives that are effective against the hepatitis C virus (Magri et al., 2015). It has broad-spectrum antiviral actions involving DNA and RNA viruses (Yu et al., 2016, 2018). Zanamivir is a strong influenza neuraminidase inhibitor (Zhao et al., 2017). It is used in combination with oseltamivir for treating drug-resistant H1N1 influenza (de Mello et al., 2018).

Theoretically, neuraminidase inhibitors are not feasible for application against SARS-CoV-2 due to the absence of a molecular target. However, the general goal in identifying a lead compound is finding a chemical structure that can theoretically match a receptor. Several neuraminidase inhibitors theoretically matched the receptor of SARS-CoV-2 PL^{PRO} and could be inhibitors of the viral protease. The presence of ACE receptor blockers among the top hits suggests that they could be used in SARS-CoV-compromised hypertensive patients. In conclusion, after a virtual screening campaign of

1697 FDA-approved drugs, 10 drugs were selected for MD and energy composition analysis. Of these, three drugs showed favorable profiles suggesting that they could be repurposed for COVID-19 treatment. The top three hits, phenformin, quercetin, and ritonavir, can be a basis for future anti-SARS CoV-2 studies.

Acknowledgements

The author acknowledges the Deanship of Scientific Research at King Faisal University for the financial support under Research Groups track (Grant No. 1811016).

Disclosure statement

No potential conflict of interest was reported by the author(s).

ORCID

Mahmoud A. A. Ibrahim  <http://orcid.org/0000-0003-4819-2040>

References

- Alfuwaires, M., Altaher, A., & Kandeel, M. (2017). Molecular dynamic studies of interferon and innate immunity resistance in MERS CoV non-structural protein 3. *Biological & Pharmaceutical Bulletin*, 40(3), 345–351. <https://doi.org/10.1248/bpb.b16-00870>
- Báez-Santos, Y. M., Mielech, A. M., Deng, X., Baker, S., & Mesecar, A. D. (2014). Catalytic function and substrate specificity of the papain-like protease domain of nsp3 from the Middle East respiratory syndrome coronavirus. *Journal of Virology*, 88(21), 12511–12527. <https://doi.org/10.1128/JVI.01294-14>
- Báez-Santos, Y. M., St. John, S. E., & Mesecar, A. D. (2015). The SARS-coronavirus papain-like protease: Structure, function and inhibition by designed antiviral compounds. *Antiviral Research*, 115, 21–38. <https://doi.org/10.1016/j.antiviral.2014.12.015>
- Bailey-Elkin, B. A., Knaap, R. C. M., Johnson, G. G., Dalebout, T. J., Ninaber, D. K., van Kasteren, P. B., Bredenbeek, P. J., Snijder, E. J., Kikkert, M., & Mark, B. L. (2014). Crystal structure of the Middle East respiratory syndrome coronavirus (MERS-CoV) papain-like protease bound to ubiquitin facilitates targeted disruption of deubiquitinating activity to demonstrate its role in innate immune suppression. *The Journal of Biological Chemistry*, 289(50), 34667–34682. <https://doi.org/10.1074/jbc.M114.609644>
- Bayly, C. I., Cieplak, P., Cornell, W., & Kollman, P. A. (1993). A well-behaved electrostatic potential based method using charge restraints for deriving atomic charges: The RESP model. *The Journal of Physical Chemistry*, 97(40), 10269–10280. <https://doi.org/10.1021/j100142a004>
- Berendsen, H. J. C., Postma, J. P. M., Gunsteren, W. F., van DiNola, A., & Haak, J. R. (1984). Molecular dynamics with coupling to an external bath. *The Journal of Chemical Physics*, 81(8), 3684–3690. <https://doi.org/10.1063/1.448118>
- Brian, D. A., & Baric, R. S. (2005). Coronavirus genome structure and replication. In *Coronavirus replication and reverse genetics* (pp. 1–30). Springer.
- Case, D. A., Betz, R. M., Cerutti, D. S., Cheatham, T. E., Darden, T. A., Duke, R. E., ... Kollman, P. A. (2016). *AMBER 2016*. University of California.
- Croxtall, J. D., & Perry, C. M. (2010). Lopinavir/Ritonavir: A review of its use in the management of HIV-1 infection. *Drugs*, 70(14), 1885–1915. <https://doi.org/10.2165/11204950-000000000-00000>
- Darden, T., York, D., & Pedersen, L. (1993). Particle mesh Ewald: An N-log(N) method for Ewald sums in large systems. *The Journal of Chemical Physics*, 98(12), 10089–10092. <https://doi.org/10.1063/1.464397>

- de Mello, C. P. P., Drusano, G. L., Adams, J. R., Shudt, M., Kulawy, R., & Brown, A. N. (2018). Oseltamivir-zanamivir combination therapy suppresses drug-resistant H1N1 influenza A viruses in the hollow fiber infection model (HFIM) system. *European Journal of Pharmaceutical Sciences*, *111*, 443–449.
- De Vivo, M., Masetti, M., Bottegoni, G., & Cavalli, A. (2016). Role of molecular dynamics and related methods in drug discovery. *Journal of Medicinal Chemistry*, *59*(9), 4035–4061. <https://doi.org/10.1021/acs.jmedchem.5b01684>
- Frisch, M. J., Trucks, G. W., Schlegel, H. B., Scuseria, G. E., Robb, M. A., Cheeseman, J. R., ... Fox, D. J. (2009). *Gaussian 09 (Version Revision E01)*. Gaussian Inc.
- Friesner, R. A., Banks, J. L., Murphy, R. B., Halgren, T. A., Klicic, J. J., Mainz, D. T., Repasky, M. P., Knoll, E. H., Shelley, M., Perry, J. K. and Shaw, D. E. (2004). Glide: a new approach for rapid, accurate docking and scoring. 1. Method and assessment of docking accuracy. *Journal of medicinal chemistry*, *47*(7), 1739–1749.
- GAFF and GAFF2 are public domain force fields and are part of the AmberTools16 distribution, a.f.d.a.h.a.o.i.a.A.M.A.t.
- Guarner, J. (2020). Three emerging coronaviruses in two decades the story of SARS, MERS, and now COVID-19. *American Journal of Clinical Pathology*, *153*(4), 420–421. <https://doi.org/10.1093/ajcp/aqaa029>
- Harcourt, B. H., Jukneliene, D., Kanjanahaluethai, A., Bechill, J., Severson, K. M., Smith, C. M., Rota, P. A., & Baker, S. C. (2004). Identification of severe acute respiratory syndrome coronavirus replicase products and characterization of papain-like protease activity. *Journal of Virology*, *78*(24), 13600–13612. <https://doi.org/10.1128/JVI.78.24.13600-13612.2004>
- Kandeel, M., & Al-Nazawi, M. (2020). Virtual screening and repurposing of FDA approved drugs against COVID-19 main protease. *Life Sciences*, *251*, 117627. <https://doi.org/10.1016/j.lfs.2020.117627>
- Kandeel, M., & Altaher, A. (2017). Synonymous and biased codon usage by MERS CoV papain-like and 3CL-proteases. *Biological & Pharmaceutical Bulletin*, *40*(7), 1086–1091. <https://doi.org/10.1248/bpb.b17-00168>
- Kandeel, M., Altaher, A., & Alnazawi, M. (2019). Molecular dynamics and inhibition of MERS CoV papain-like protease by small molecule imidazole and aminopurine derivatives. *Letters in Drug Design & Discovery*, *16*(5), 584–591. <https://doi.org/10.2174/1570180815666180918161922>
- Kandeel, M., Ibrahim, A. A., Fayed, M., & Al-Nazawi, M. (2020). From SARS and MERS CoVs to SARS-CoV-2: Moving toward more biased codon usage in viral structural and non-structural genes. *Journal of Medical Virology*, *92*(6), 660–666. <https://doi.org/10.1002/jmv.25754>
- Kandeel, M., Yamamoto, M., Al-Taher, A., Watanabe, A., Oh-Hashi, K., Park, B. K., Kwon, H.-J., Inoue, J.-i., & Al-Nazawi, M. (2020). Small molecule inhibitors of Middle East respiratory syndrome coronavirus fusion by targeting cavities on heptad repeat trimers. *Biomolecules & Therapeutics*, <https://doi.org/10.4062/biomolther.2019.202>
- Kerrigan, J. E. (2013). Molecular dynamics simulations in drug design. In Sandhya Kortagere (Ed.), *In Silico models for drug discovery* (pp. 95–113). Humana Press.
- Lei, J., Mesters, J. R., Drosten, C., Anemüller, S., Ma, Q., & Hilgenfeld, R. (2014). Crystal structure of the papain-like protease of MERS coronavirus reveals unusual, potentially druggable active-site features. *Antiviral Research*, *109*, 72–82. <https://doi.org/10.1016/j.antiviral.2014.06.011>
- Lim, J., Jeon, S., Shin, H. Y., Kim, M. J., Seong, Y. M., Lee, W. J., Choe, K. W., Kang, Y. M., Lee, B., & Park, S. J. (2020). Case of the Index patient who caused tertiary transmission of coronavirus disease 2019 in Korea: The application of lopinavir/ritonavir for the treatment of COVID-19 pneumonia monitored by quantitative RT-PCR. *Journal of Korean Medical Science*, *35*(7), e89. <https://doi.org/10.3346/jkms.2020.35.e89>
- Liu, Z., Xiao, X., Wei, X., Li, J., Yang, J., Tan, H., Zhu, J., Zhang, Q., Wu, J., & Liu, L. (2020). Composition and divergence of coronavirus spike proteins and host ACE2 receptors predict potential intermediate hosts of SARS-CoV-2. *Journal of Medical Virology*, *92*(6), 595–601. <https://doi.org/10.1002/jmv.25726>
- Magri, A., Reilly, R., Scalacci, N., Radi, M., Hunter, M., Ripoll, M., Patel, A. H., & Castagnolo, D. (2015). Rethinking the old antiviral drug moroxydine: Discovery of novel analogues as anti-hepatitis C virus (HCV) agents. *Bioorganic & Medicinal Chemistry Letters*, *25*(22), 5372–5376. <https://doi.org/10.1016/j.bmcl.2015.09.029>
- Maier, J. A., Martinez, C., Kasavajhala, K., Wickstrom, L., Hauser, K. E., & Simmerling, C. (2015). ff14SB: Improving the accuracy of protein side chain and backbone parameters from ff99SB. *Journal of Chemical Theory and Computation*, *11*(8), 3696–3713. <https://doi.org/10.1021/acs.jctc.5b00255>
- Massova, I., & Kollman, P. (2000). Combined molecular mechanical and continuum solvent approach (MM-PBSA/GBSA) to predict ligand binding. *Perspectives in Drug Discovery and Design*, *18*(1), 113–135. <https://doi.org/10.1023/A:1008763014207>
- Mielech, A. M., Kilianski, A., Baez-Santos, Y. M., Mesecar, A. D., & Baker, S. C. (2014). MERS-CoV papain-like protease has deISGylating and deubiquitinating activities. *Virology*, *450–451*, 64–70. <https://doi.org/10.1016/j.virol.2013.11.040>
- Ratia, K., Kilianski, A., Baez-Santos, Y. M., Baker, S. C., & Mesecar, A. (2014). Structural basis for the ubiquitin-linkage specificity and deISGylating activity of SARS-CoV papain-like protease. *PLoS Pathog*, *10*(5), e1004113.
- Shi, J., Zhang, J., Li, S., Sun, J., Teng, Y., Wu, M., Li, J., Li, Y., Hu, N., Wang, H., & Hu, Y. (2015). Epitope-based vaccine target screening against highly pathogenic MERS-CoV: An in silico approach applied to emerging infectious diseases. *PLoS One*, *10*(12), e0144475 <https://doi.org/10.1371/journal.pone.0144475>
- WHO (2020). <https://www.who.int/emergencies/diseases/novel-coronavirus-2019>.
- Yang, X., Chen, X., Bian, G., Tu, J., Xing, Y., Wang, Y., & Chen, Z. (2014). Proteolytic processing, deubiquitinase and interferon antagonist activities of Middle East respiratory syndrome coronavirus papain-like protease. *J. Gen. Virol*, *95*(Pt 3), 614–626. <https://doi.org/10.1099/vir.0.059014-0>
- Yu, X.-B., Chen, X.-H., Ling, F., Hao, K., Wang, G.-X., & Zhu, B. (2016). Moroxydine hydrochloride inhibits grass carp reovirus replication and suppresses apoptosis in Ctenopharyngodon idella kidney cells. *Antiviral Research*, *131*, 156–165. <https://doi.org/10.1016/j.antiviral.2016.05.008>
- Yu, X.-B., Hao, K., Li, J., Chen, X.-H., Wang, G.-X., & Ling, F. (2018). Effects of moroxydine hydrochloride and ribavirin on the cellular growth and immune responses by inhibition of GCRV proliferation. *Research in Veterinary Science*, *117*, 37–44. <https://doi.org/10.1016/j.rvsc.2017.11.007>
- Zhao, T.-F., Qin, H.-J., Yu, Y., Yang, M.-B., Chang, H., Guo, N., He, Y., Yang, Y., & Yu, P. (2017). Multivalent zanamivir-bovine serum albumin conjugate as a potent influenza neuraminidase inhibitor. *Journal of Carbohydrate Chemistry*, *36*(4–6), 235–246. <https://doi.org/10.1080/07328303.2017.1390577>